Journal of Environmental Protection, 2011, 2, 828-839
doi:10.4236/jep.2011.26094 Published Online August 2011 (http://www.SciRP.org/journal/jep)

Experimental and Numerical Investigation of Desalination Plant Outfalls in Limited Disposal Areas

Mohamed E. Abou-Elhaggag[1*], Mohamed H. El-Gamal[1], Mohamed I. Farouk[2]

[1]Faculty of Engineering, Cairo University, Giza, Egypt; [2]Faculty of Engineering, Ain Shams University, Cairo, Egypt.
Email: mohamedelgamal@yahoo.com

Received May 19th, 2011; revised June 21st, 2011; accepted July 25th, 2011.

ABSTRACT

In this study, experimental and numerical investigations of the dense brine jets are conducted for disposal areas of limited extent. First, a new experimental model representing a section of sea floor with a single port brine outfall is built to study different characteristics of dense jets. Second, a number of numerical experiments have been conducted via Fluent CFD package to compare the numerical results with its corresponding physical observations and measurements. Experimental observations are made for both the terminal height of rise of dense jets discharged vertically from circular outlets into calm and homogeneous environment and for concentration profiles along the dense jet trajectory. Various combinations of port diameters and concentration of effluent salinities are investigated to cover a wide range of conditions. The results from the carried out experiments are compared to different available experimental and field observations from the literature. A new model for the terminal height of rise of dense jets has been derived. The experimental observations of concentrations along the dense jet trajectory are analyzed to quantify the mixing patterns for a given operating condition from the source point to the terminal height of rise. The numerical model has been used to identify the penetration depth and also to get the temporal variation of the brine breakthrough curves at different locations above the disposal port. The numerical model has shown the existence of multipeak breakthrough curves for the farest points from the port (*but the closest to the water free surface*).

Keywords: *Desalination*, *Dense Jets*, *Plumes*, *Terminal Height*, *Densimetric Froude Number*, *Fluent*

1. Introduction

Due to the limited fresh water resources in many countries all over the world, desalination industry has been widely flourished within its countries. It is expected that the global desalinated water supply will reach 54 billion m3 per year by 2020 [1]. It has been also noted that 24% of the world desalination capacity occurs in Saudi Arabia. Moreover, the Middle East houses the largest reverse osmosis facility in world.

All desalination processes involve three liquid streams: the saline feedwater stream (brackish or seawater), the low-salinity product water, and the very saline concentrate (brine or reject water) stream. A by-product of desalination is brine which is a concentrated salt solution (with more than 35 000 mg/1 dissolved solid) that must be disposed of; generally by discharge it into deep saline aquifers or into oceans or seas via outfalls.

For seawater desalination plants, it seems natural and practical to dispose their brine waste back to the sea, via marine outfalls at some distance from the shoreline [2]. Marine outfalls are considered the most feasible option for brine disposal from seawater desalination plants due to their reduced implementation uncertainty, well-supported technology, minimized land take, ability to monitor and control, minimized maintenance and operation fess [3]. The marine outfall might be surface discharge, or single port outfall or multiport diffusers. Modern, large capacity plants require submerged discharges, in form of a negatively buoyant jet, that ensure a high dilution in order to minimize harmful impacts on the marine environment [4].

The impact of brine disposal operations on coastal and marine environment is still largely unknown; however, it is commonly thought that the brines discharged must ultimately be diluted and transported before disposed to

the sea. Nevertheless, for each coastal seawater desalination plant, care has always been taken to determine the optimum site of water intakes and brine waste outfalls. Brine disposal has the potential to degrade the physical, chemical and biological characteristics of the receiving water body [5]. The degree of degradation is highly dependent on the total volume of the brine being released, its characteristics, the dilution rate prior to discharge, and the characteristics of the receiving waters. The effect of the brine on the environment is also highly dependent on the geometric installation of the discharge outfall. Several studies have shown the effect of the brine disposal on the biophysical coastal environment [6-9]. Therefore, it is important to understand how brine is dispersed into the sea, so that we can minimize its potential environmental impact.

Many experimental and field studies were conducted to study the hydraulics of dense jets and plumes related to the outfalls of the desalination plants, especially the determination of the terminal height of rise, jets trajectory, and concentrations profiles. The pioneer study by [10] who investigated experimentally the jets in stagnant fluids with different inclination angles of 30˚, 45˚, 60˚, and 90˚ above the horizontal. Further experimental studies by [11-13] investigated jet trajectories and mixing under both stagnant and flowing conditions. In more recent experiments, [14] have investigated the 30˚, 45˚ and 60˚ configuration limiting the measurements to jet trajectories without consideration of dilution values. All these studies predict only near-field (initial mixing until impingement with boundary) characteristics and did not include the intermediate-field (boundary interaction and density current development) or far-field characteristics (density currents and passive mixing and transport) of the brine [4].

Modeling the environmental impacts of brine waste discharges into the sea is a difficult and a complex task. The difficulties arise from the variety and variability of the mixing processes that subsequently dilute, spread and transport the brine plume. Dynamic nature of the marine environment (currents, waves, and tides), static conditions of disposal site (depth, bottom slope), the configuration of the marine outfall (number of ports, port diameter, inclination and riser height), ambient and brine waste physical and chemical characteristics are among factors that should be considered for accurate simulation of outfall operation. Currently, no flexible and widely validated predictive tool exists to deal with the special geometrical aspects of such brine discharges, encompassing both the initial negatively buoyant free jets and the final bottom density current plumes [4].

Given the scarcity of reliable experimental data (notably dilution measurements) for the entire negatively buoyant jet, a program of experimental studies supported by detailed computational fluid dynamics (CFD) modeling, appears to be crucial in view of ongoing design and sitting activities for numerous new desalination plants all around the globe. The study in hand presents the outcomes of laboratory experiments of submerged negatively buoyant jet discharging over a flat bottom in a calm ambient environment to investigate the jet trajectory and dilution. The study is supported by numerical investigation of the jet dilution and trajectory using the state of the art Fluent CFD package.

2. Previous Experimental Studies on Outfalls Characteristics

The prediction of brine jet characteristics relies heavily upon semi-empirical formulations. These formulas show that the vertical extent of the jet is dependent upon the jet velocity, port diameter, and the density ratio between the ambient and effluent fluids and the dilution of the jet is dependent on the port velocity and geometric parameters as well as the ambient current velocity. **Table 1** presents a list of the developed semi-empirical formula from previous studies.

There are significant variations in the reported results of the experimental and field studies concerning negatively buoyant jet. Some variations may be attributed to: the methods adopted in defining and measuring maximum jet height, the effect of Reynolds number, the effect of relative density difference, and the effect of mass flux. Accordingly, the objective of this study is to conduct experimental and numerical study for the negative dense jets. The objective of the experimental investigation is to reproduce a number of lab experiments for the negative dense jets so as to be sure of all the jet and ambient parameters then to conduct a numerical analysis for some selected cases of the lab experiments and to compare the results

Table 1. Summary of some of the previous studies on dense jet problem.

No.	Ref.	Exp./Field	Z_m
1	Turner, 1966 [15]	Exp	$Z_m/r = 2.46F_r$
2	Abraham, 1967 [16]	Exp	$Z_m/r = 2.74F_r$
3	Cederwal, 1968 [17]	Exp	$Z_m/r = 4.59(F_r)^{0.67}$
4	Fan *et al.*,1969 [18]	Exp	$Z_m/r = 2.68F_r$
5	Zeitoun, 1970 [19]	Exp	$Z_m/r = 2.43F_r$
6	Holly, 1972 [20]	Exp	$Z_m = (3.4 \times 10^{-0.148Fe})F_r$
7	Chu, 1974 [21]	Math	$Z_m = 1.14L_m(L_m/L_b)^{1/3}$
8	Tong, 1979 [22]	Exp	$Z_m = 1.7V_o(D_o/g')$
9	James, 1983 [23]	Exp	$Z_m/r = 2.57F_r$
10	Mcllelan, 1986 [24]	Field	$Z_m/r = 3.11F_r$
11	El-Damak, 1990 [25]	Exp	$Z_m/r = 3.11F_r^{6/16}$
12	Roberts, 1997 [26]	Exp	$Z_m/r = 3.11F_r$ ($\theta = 60^o$)
13	Zhang, 1998 [27]	Exp	$Z_m/r = 3.06F_r$
14	Pantokratoras, 1999 [28]	Exp	Y_m/D_o =1.74 Sin $(\theta_o)^{1.53}$

3. Dimensional Analysis

Consider a miscible jet of dense fluid issuing vertically from a round source in a homogeneous and calm environment. The maximum vertical penetration, Z_m of the jet is dependent on variables that characterize the source conditions. A general functional relationship for the dependent variable Z_m is:

$$Z_m = f\left(Q_o, M_o, B_o\right) \quad (1)$$

where:

Q_o the jet outlet mass flux = ($\pi r^2 V$);
M_o the momentum flux = ($\pi r^2 V^2$),
B_o the buoyancy flux = ($\pi r^2 V \Delta\rho/\rho_a$),
r the radius of the jet port,
ρ_a the density of the ambient fluid,
$\Delta\rho$ the density difference between the ambient fluid and the jet &
V the fluid average velocity at the port's outlet.

For small distances from the nozzle the volume flux of the entrained ambient fluid becomes approximately equal to the initial volume flux so that the initial volume flux becomes dynamically unimportant and may be ignored [27]. Thus, it can be deduced from dimensional analysis that:

$$Z_m = C_o M_o^{3/4} B_o^{-1/2} = C_m r F_r \quad (2)$$

where:

C_o & C_m constants that must be determined from experiments &
F_r the jet densimetric Froude number.

As shown in the previous studies, the maximum penetration for a point source is linearly proportional to F_r. This fundamental property has been used to analyze & to determine the constant C_m. The values of densimetric Froude number can be plotted against the values of the dimensionless quantity Z_m/r for the different sets of experimental observations.

4. Experimental Investigation

4.1. Experimental Setup

A 1:10 physical model of limited extent and dimensions was built at the Irrigation and Hydraulics laboratory, Faculty of Engineering, Cairo University. The model reproduces prototype dimensions of 12.0 m long and 6.0 m wide with a water depth of 6.0 m. The model scale was selected such that the penetration of the dense effluent jet does not exceed the model boundaries.

A stagnant fresh water is used as a fluid ambient (corresponds to seawater in the prototype); while salt and dye are mixed with freshwater in a holding tank to represent the dense brine and the mix is pumped through the jet port. Various model ports' diameters were tested. The tested model diameters correspond to (5.0, 10.0 & 15.0 cm) diameters in the prototype scale. A wide range of prototype velocities were tested in the model, the tested velocity range corresponds to prototype velocities from 0.46 to 4.0 m/sec.

Figure 1 shows the different elements of the laboratory setup of the dense jet model experiment. Among these elements are:

1) Fresh water tank (FWT),
2) Salt water tank (SWT),
3) Auxiliary water tank,
4) Pump and motor,
5) Fitting and valves,
6) Nozzles,
7) Samples extraction mechanism,
8) Temperature conductivity meter,
9) Sensitive scale,
10) Calibrated containers &
11) Dye injection system.

4.2. Experimental Procedure

The dense jet experiment is carried out by discharging saltwater into a transparent tank filled with fresh water to produce the required difference in density between the discharged dense jet and the ambient fresh water. The amount of salt (NaCl) required to produce the density difference for a given test is determined by weight and checked using the temperature conductivity meter. The temperatures of the fresh water and saltwater were practically identical and close to room temperature to minimize thermal effects on the flow. During a test, the saltwater is discharged from SWT to the FWT at a constant flow rate, which was controlled by keeping constant difference in head between water levels in FWT and the

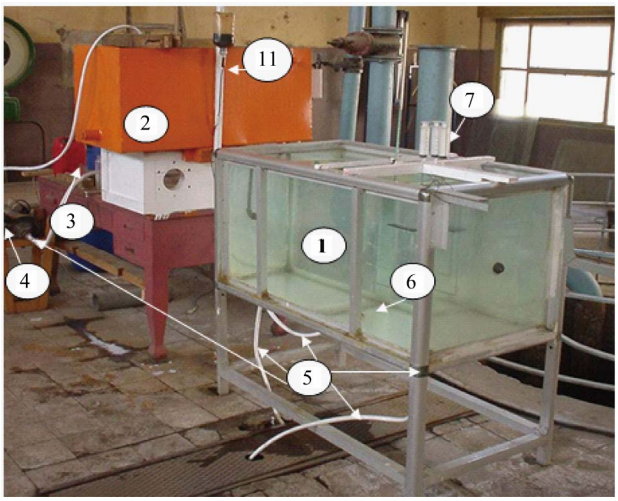

Figure 1. A photograph of the experimental setup with limited extent.

SWT using overflows arrangements in both tanks, in addition to a control valve.

Nine series of model tests were conducted to investigate both small and large densimetric Froude number jets, while maintaining turbulent flow conditions at the exit. The nine series of tests cover the following ranges: three port diameters (5 mm, 10 mm, and 15 mm) with three different values of salinity that cover a broad range of conditions (5000 ppm, 10000 ppm, 30000 ppm), **Table 2**.

4.3. Jet Structure

When the discharge valve is suddenly opened at the beginning of the test, the initial development of the jet is characterized by the formation of a turbulent front that moved upward and then collapsed. After the collapse of the starting front, the height of the jet fluctuates with time, as noted in previous studies. At small densimetric Froude number the fluctuations are small and the jet penetration is stable. The amplitude of the jet height fluctuation increased with the increase of the densimetric Froude number. A vertical gauge mounted in the fresh water tank is used to measure the jet penetration above the nozzle. The maximum jet penetration, Z_m, is determined as an average of three consecutive maximum jet heights attained after the collapse of the starting front. Dye was injected to enhance the visibility in the fresh water tank. **Figure 2** presents two photographs of negatively buoyant jets discharged vertically in calm and homogenous environment. They are captured during the test series 4. The densimetric Froude numbers for the jets in **Figure 2** are 28.0 and 33.8 respectively and the average steady maximum penetration depths are 20 and 23.5 cm respectively.

4.4. Sampling Process of Concentrations along Dense Jet Trajectory

In order to measure the concentration along the jet, a number of sampling points extracting from different heights above the port is constructed. For each test, water samples along the jet trajectory are extracted using the samples extraction mechanism for the determination of the dilution or salinity profile along the jet trajectory. For observations in which the maximum jet penetration is small and below the considered sampling point, only the first sample close to the nozzle is extracted according to the maximum jet penetration. The conductivity of the different samples is determined for each test using the temperature conductivity probe.

Table 2. Summary of tested conditions.

Test Series	r (mm)	$\Delta\rho/\rho$	F_r
1	2.5	0.00346	28 - 64.5
2	5	0.00346	23 - Dec
3	7.5	0.00353	4.2 - 15.8
4	2.5	0.00736	23.9 - 59.4
5	5	0.00736	11.7 - 31.8
6	7.5	0.0074	4.2 - 16.2
7	2.5	0.0224	17.4 - 56.9
8	5	0.0224	12.3 - 24.5
9	7.5	0.0224	6.5 - 11.1

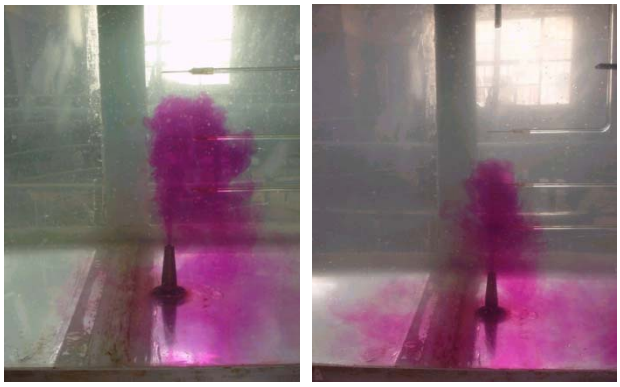

(a) (b)

Figure 2. Jet Structure of Dense Jets for Port Diameter 5mm. (a) F_r = 33.8 & Z_m = 23.5cm; (b) F_r = 28 Z_m = 20 cm.

4.5. Jet Velocity at Port End

One of the most important observed parameters in the dense jet experiment is the jet velocity at port surface. The volume-time approach is used to determine the discharge through the jet ports. The jet velocities are determined by dividing the discharge by the cross sectional area of the nozzle and the average value for jet velocities are used in further analysis.

5. Results of Laboratory Experimental Observations

Figure 3 summarizes the results of all the experimental lab observations as per the conducted 9 test series in this study (refer to **Table 2**). The figure presents a relation between the densimetric Froude number and the normal-

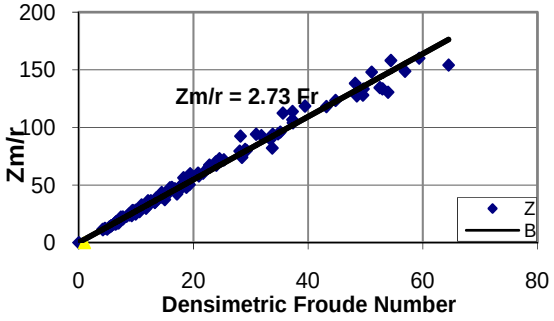

Figure 3. Densimetric froude number versus Z_m/r for the whole sets of experimental observations (current study).

ized penetration depth It is noted that this relation is almost linear and can be closely approximated using a straight line. The best linear fit for all of the observations takes the following form:

$$Z_m / r = 2.73 F_r \quad (3)$$

6. Comparison with Previous Empirical and Analytical Results

The pre-mentioned procedure in the analysis of terminal height of rise is followed again using different sources of data from previous studies. The new sets of data represent both experimental observations and field observations at a location of brine outfall. Data used in this part of the analysis include:

- Experimental observations by [23].
- Field observations by [24]
- Experimental observations by [25]
- Experimental observations by [27]
- Experimental observations by [29].

It should be mentioned that this is the first time (to the authors' knowledge) the combination of different sets of data is used in a similar analysis. The different data groups are rearranged in a form suitable for the intended analysis. The dimensionless densimetric Froude number is plotted against the dimensionless quantity Z_m/r. **Figure 4** represents the mentioned plot with densimetric Froude number on the horizontal axis and Z_m/r on the vertical axis.

It is clear from **Figure 4** the common trend among different sets of data especially the current experimental observations, [23,27]

It has been noted that the models derived by [17] and [25] seem to be outliers compared to other models. It has been noted that some data [25] shows larger scatter than other groups of data, and it is worth noting that some of these observations are omitted from the current analysis as it looks to be far away from the common trend among different groups of data.

The results of [18] for the constant of proportionality (Cm = 2.68) were based on measurements of negatively buoyant jets in calm atmospheric conditions. Most studies conducted by [27] focused on discharges inclined to the horizontal. His results in this field have a valuable weight in dense jet problems, but in case of vertically upward jets the result by [27] for the constant of proportionality (Cm = 2.43) underestimate the terminal height of rise. The results by [23] for the constant of proportionality (Cm = 2.5) were obtained based on certain conditions for H/d ratios (Riser height/water depth). The study by [15] is valuable because it is one of the first experimental studies on negatively buoyant discharges however, the constant of proportionality (Cm = 2.46) was

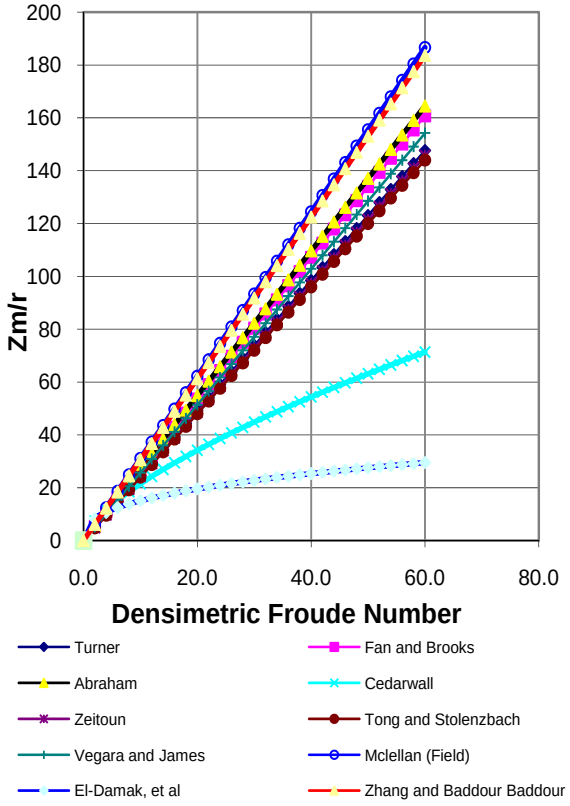

Figure 4. Comparison among previous results.

proved by following studies to underestimate the terminal height of rise. The experimental study by [15] yields a constant of proportionality (Cm = 2.40), this may be attributed to the introduction of cross flow condition in the experiments. It is worth to remember that all the previous results are derived based on single group of observations by the individual researcher. While in this study the obtained results are based on different sets of data that cover a wide range of conditions.

The results obtained using field data [24] yield the largest constant of proportionality Cm = 3.11. Thus the larger predictions of the measurements may be attributed due to the measurements techniques (acoustic measurements) and the variability in the ocean environment. The results obtained by [27] based on experimental study yield a constant of proportionality Cm = 3.06. This may be attributed to the small number of observed data points, 22 observations that were used to estimate the constant of proportionality. In addition to the exclusions of small Densimetric Froude number observations (Fr < 7) that might decrease the constant of proportionality.

Figure 5 is the same as **Figure 4** after excluding the above mentioned studies and after including the current experimental study. The line producing the best fit of the different groups of data is plotted also on **Figure 5** and is

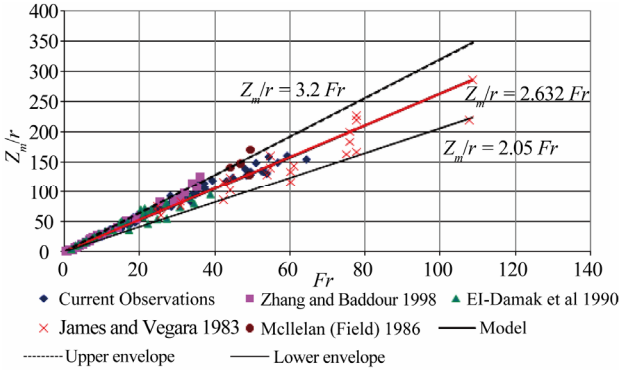

Figure 5. Terminal height of rise for different groups of data.

also given in Equation (4) below. The constant, C takes a value of 2.63 and the equation that simulates the terminal height of rise of negatively buoyant plumes discharged vertically in homogeneous and calm environment takes the following form:

$$Z_m/r = 2.63F_r \tag{4}$$

The scatter of the data points around the straight line is expected because of the wide range of covered parameters. It has been noted that the average error between the predicted values using Equation (3) and Equation (4) is found to be about 10%. The upper and lower envelopes based on the different data sets are also plotted on the figure.

It might be recommended that designer could depend on Equation (4) which is based on the whole observed data to represent the maximum jet height of a negatively buoyant effluent. Equation (4) provides a method of balancing port diameter, total dense effluent flow, and relative density difference to obtain a desired maximum jet height. And can be used for design issues.

7. Numerical Experiments

7.1. The Theoretical Approach of the CFD Package:

FLUENT [30] is one of the CFD commercial packages that are commonly used for studying the hydrodynamics of complicated flow fields including multiphase flow applications. In the study in-hand, FLUENT package [30] is adopted for carrying out all numerical simulations. This problem is considered as one of the most sophisticated problems of fluid dynamics, where it considers a multi-phase unsteady turbulent flow.

To change from a single-phase model, where a single set of conservation equations for momentum and continuity is solved, to a multi-phase model, additional sets of conservation equations must be introduced. In the process of introducing additional sets of conservation equations, the original set must also be modified.

Since the problem is solved as unsteady flow, the equation is updated each time step, which is taken 0.2 sec in this problem. The governing equations are solved sequentially for this numerical simulation, because the equations are nonlinear.

Turbulent flows are characterized by fluctuating velocity fields. These fluctuations mix transported quantities such as momentum, energy, and species concentration, and cause the transported quantities to fluctuate as well. Since these fluctuations in this case study were of small scale and high frequency, they were too computationally expensive.

The description of discussed multi-phase flow as interpenetrating continua incorporates the concept of phases volume fractions, denoted here by α_q. Volume fractions represent the space occupied by each phase, and the laws of conservation of mass and momentum are satisfied by each phase individually. The derivation of the conservation equations can be done by ensemble averaging the local instantaneous balance for each of the phases or by using the mixture theory approach.

The volume of phase q, V_q, is defined by

$$V_q = \int_v \alpha_q \mathrm{d}V \tag{5}$$

where

$$\sum_{q=1}^{2} \alpha_q = 1 \tag{6}$$

The effective density of phase q is

$$\hat{\rho}_q = \alpha_q \rho_q \tag{7}$$

where

ρ_q The physical density of phase q.

Conservation of Mass

The general form of the conservation of mass equation for phase q is

$$\frac{\partial}{\partial t}\left(\alpha_q \rho_q\right) + \nabla \cdot \left(\alpha_q \rho_q \boldsymbol{\upsilon}_q\right) = \sum_{p=1}^{n} \dot{m}_{pq} \tag{8}$$

where

$\boldsymbol{\upsilon}_q$ The velocity of phase q

$\dot{m}_{pq}$ Characterizes the mass transfer from the p^{th} to q^{th} phase.

From the mass conservation once can obtain

$$\dot{m}_{pq} = -\dot{m}_{qp} \tag{9}$$

$$\dot{m}_{pp} = 0 \tag{10}$$

The continuity equation for the studied multi-phase problem, as solved by [23], is presented here for the general case of a multi-phase flow. The volume fraction of

each phase is calculated from a continuity equation:

$$\frac{\partial}{\partial t}\left(\alpha_q\right)+\nabla\cdot\left(\alpha\boldsymbol{\upsilon}_q\right)=\frac{1}{\rho_q}\left(\sum_{p=1}^{2}\dot{m}_{pq}-\alpha_q\frac{\mathrm{d}_q\rho_q}{\mathrm{d}t}\right) \quad (11)$$

The solution of this equation for each secondary phase, along with the condition that the volume fractions sum to one (given by Equation (8)), allows for the calculations of the primary-phase volume fraction.

Conservation of Momentum

The general form of the conservation of momentum equation

$$\begin{aligned}&\frac{\partial}{\partial t}\left(\alpha_q\rho\boldsymbol{\upsilon}_q\right)+\nabla\cdot\left(\alpha_q\rho_q\boldsymbol{\upsilon}_q\boldsymbol{\upsilon}_q\right)\\&=\alpha_q\nabla p+\nabla\cdot\overline{\overline{T}}_q+\sum_{p=1}^{2}\left(\boldsymbol{R}_{pq}+\dot{m}_{pq}\boldsymbol{\upsilon}_{pq}\right)\\&+\alpha_q\rho_q\left(\boldsymbol{F}_q+\boldsymbol{F}_{lift,q}+\boldsymbol{F}_{vm,q}\right)\end{aligned} \quad (12)$$

where

$\overline{\overline{T}}_q$ is the q^{th} phase stress-strain tensor

$$\overline{\overline{T}}_q=\alpha_q\mu_q\left(\nabla\boldsymbol{\upsilon}_q+\boldsymbol{\upsilon}_q^T\right)+\alpha_q\left(\lambda_q-\frac{2}{3}\mu_q\right)\nabla\cdot\boldsymbol{\upsilon}_q\overline{\overline{I}} \quad (13)$$

The conservation of momentum equation for the studied multi-phase flows, as solved by [30], is presented here for the general case of a multi-phase flow. The conservation of momentum for a fluid q is

$$\begin{aligned}&\frac{\partial}{\partial t}\left(\alpha_q\rho_q\boldsymbol{\upsilon}_q\right)+\nabla\cdot\left(\alpha_q\rho_q\boldsymbol{\upsilon}_q\boldsymbol{\upsilon}_q\right)\\&=\alpha_q\nabla p+\nabla\cdot\overline{\overline{T}}_q+\alpha_q\rho_q\boldsymbol{g}+\alpha_q\rho_q\left(\left(\boldsymbol{F}_q+\boldsymbol{F}_{lift,q}+\boldsymbol{F}_{vm,q}\right)\right)\\&+\sum_{p=1}^{2}\left(K_{pq}\left(\boldsymbol{\upsilon}_p\boldsymbol{\upsilon}_q\right)+\dot{m}_{pq}\boldsymbol{\upsilon}_{pq}\right)\end{aligned} \quad (14)$$

The conservation of momentum for the fluid phases is similar to Equation (23), and that for the "*s*" solid phase is

$$\begin{aligned}&\overline{\overline{T}}_q=\alpha_q\mu_q\left(\nabla\boldsymbol{\upsilon}_q+\boldsymbol{\upsilon}_q^T\right)+\alpha_q\left(\lambda_q-\frac{2}{3}\mu_q\right)\nabla\cdot\boldsymbol{\upsilon}_q\overline{\overline{I}}\\&\frac{\partial}{\partial t}\left(\alpha_s\rho_s\boldsymbol{\upsilon}_s\right)+\nabla\cdot\left(\alpha_s\rho_s\boldsymbol{\upsilon}_s\boldsymbol{\upsilon}_s\right)\\&=\alpha_s\nabla p\nabla p_s+\nabla\cdot\overline{\overline{T}}_s+\alpha_s\rho_s\boldsymbol{g}+\alpha_s\rho_s\left(\left(\boldsymbol{F}_s+\boldsymbol{F}_{lift,s}+\boldsymbol{F}_{vm,s}\right)\right)\\&+\sum_{l=1}^{2}\left(K_{ls}\left(\boldsymbol{\upsilon}_l\boldsymbol{\upsilon}_s\right)+\dot{m}_{ls}\boldsymbol{\upsilon}_{ls}\right)\end{aligned} \quad (15)$$

Euler's equation was applied to sort out the above equations.

7.2. The 3D Numerical Model Development and Boundary Conditions

The case study in-hand is an unsteady multiphase turbulent flow. A three dimensional model was constructed for this regard using Fluent package. The model boundary conditions are as follow: the bed side is assumed wall boundary. The inlet velocity plan is located 5cm above the bed levels. Due to the model tank symmetry, the symmetrical option is used in both directions and thus one fourth the model domain is simulated to minimize the number of nodes and elements as shown in **Figure 6**. The model comprises 94,684 tetrahedral cells and 184,977 triangular interior faces as shown in **Figure 7**, which was created by [31].

Two different densities, 1.00346 ρ_w & 1.00736 ρ_w are assumed in this study, where three inlet velocities are assumed for each density. One inlet diameter (r = 0.05 m, is assumed in all studied runs, refer to **Table 3**.

7.3. Results of the Numerical Investigations

Figures 8-13 illustrate the results of the six numerical

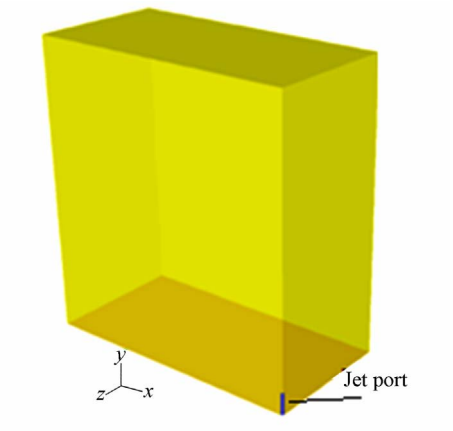

Figure 6. The numerical model (one fourth of the domain).

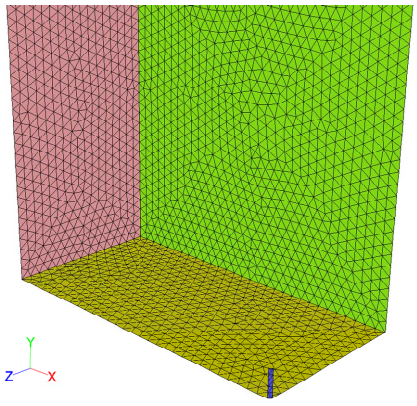

Figure 7. The numerical mesh.

Table 3. List of conducted numerical experiments.

Numerical Run #	(mm)	Jet Density	Jet Velocity (m/s)
1	5	$1.00346\rho_w$	0.2211
2	5	$1.00346\rho_w$	0.424
3	5	$1.00346\rho_w$	0.8403
4	5	$1.00736\rho_w$	0.3144
5	5	$1.00736\rho_w$	0.5844
6	5	$1.00736\rho_w$	1.1485

Table 4. Comparison of numerical results with semi-empirical formulas.

Run #	Penetration Depth (m)			
	Numerical	Equation (4)	Min. Envelop*	Max. Envelop[a]
1	0.164	0.1639	0.123	0.192c
2	0.314	0.314	0.236	0.368
3	0.547	0.6226	0.4675	0.7298
4	0.155	0.1597	0.1199	0.1872
5	0.292	0.2969	0.2229	0.348
6	0.513	0.5834	0.4381	0.6839

[a]For minimum and maximum envelops, refer to **Figure 5**.

runs as shown in **Table 3** respectively. Four brine concentration ratios are shown in each Figure, which are 50%, 20%, 10% & 1%. The maximum penetration height is assumed to be equal to brine concentration ratio 1%. The results show that, when the brine is lighter, it reaches its maximum height quicker before it spreads horizontally as shown in **Figures 8-10**. **Table 4** presents all numerical results. The table also compares the results with the empirical equations (Equation 4) and the upper and lower envelops identified in **Figure 5**. **Figure 14** illustrate the velocity vectors for one of the numerical runs. It is worth to be noted that all the numerical results are bounded by the upper and lower envelops identified in **Figure 5**.

7.4. The Brine Breakthrough Curves (Concentration with Time)

One of the advantages of using numerical simulation is developing the relation between the brine concentration ratio and the time. **Figures 15** and **16** represent the temporal variation of the brine concentration with the course of time for an example run (run No.5) where the maximum penetration height is 29.2 cm. The brine concentration breakthrough curve is given every 2 cm. **Figure 15** represents the breakthrough curves for vertical heights from 2 cm to 14 cm measured from the port, whereas **Figure 16** gives the corresponding brine breakthrough curves for heights from 16 cm to 28 cm.

Examination of the simulated breakthrough curves shows a number of interesting issues that can be summarized as follow: It has been noted that the peak concentration values of the breakthrough curves decrease with the depth and these peak values start to decrease with the course of time due to the continuous water entrainment

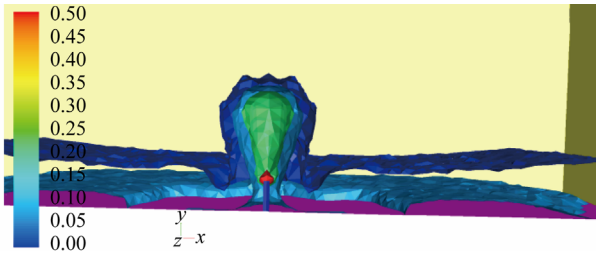

Figure 8. (penetration height = 0.164 m, Run No. 1) v = 0.2211 m/s, d = 0.1 & density = 1.00346 ρ_w.

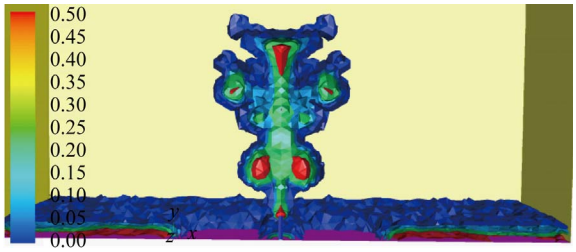

Figure 9. (penetration height = 0.314 m, Run No. 2), v = 0.424 m/s, d = 0.1 m & density = 1.00346 ρ_w.

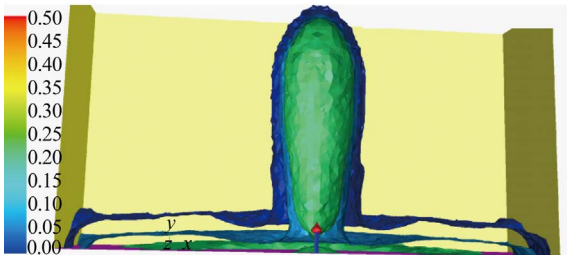

Figure 10. (penetration height = 0.547 m, Run No. 3), v = 0.8403 m/s, d = 0.1 m & density =1.00346 ρ_w.

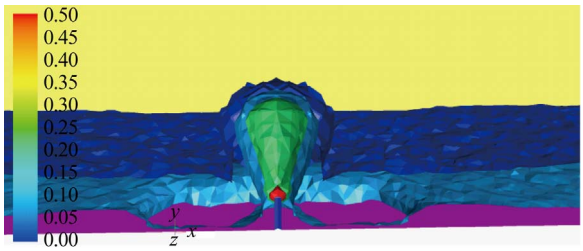

Figure 11. (penetration height = 0.155 m, Run No. 4), v = 0.3144 m/s, d = 0.1 m & density 1.00736 ρ_w –.

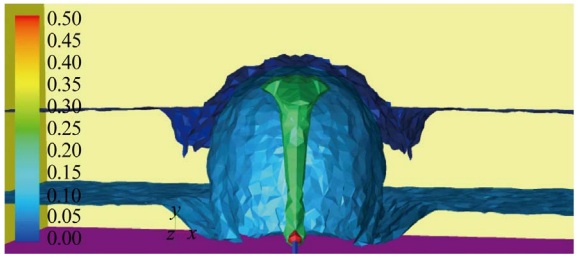

Figure 12. (penetration height = 0.292 m, Run No. 5), v = 0.5834 m/s, d = 0.1 m & density = 1.00736 ρ_w –.

from the water body outside the buoyant jet. It has been also noted that the rate of brine dilution (dC_r/dt, where C_r is the concentration ratio) is relatively large just after reaching the peak value and this rate starts to decrease significantly afterward (**Figure 15**). The significant reduction in the dilution rate could be due to the limited control water volume around the tested jet.

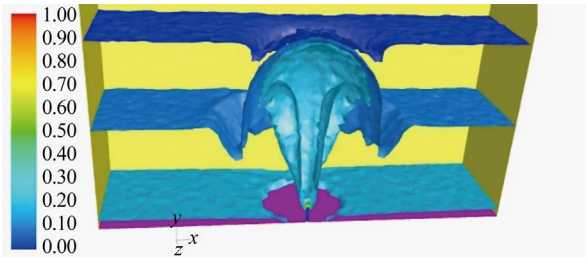

Figure 13. (penetration height = 0.513 m, Run No. 6), v = 1.1485 m/s, d = 0.1 m & density = 1.00736 ρ_w.

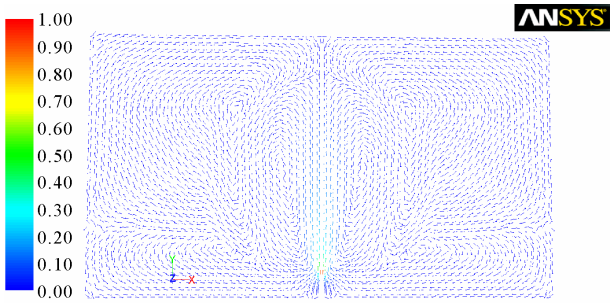

Figure 14. Velocity vector for Run No. 6 (v = 1.1485 m/s, d = 0.1 m & density 1.00736 ρ_w).

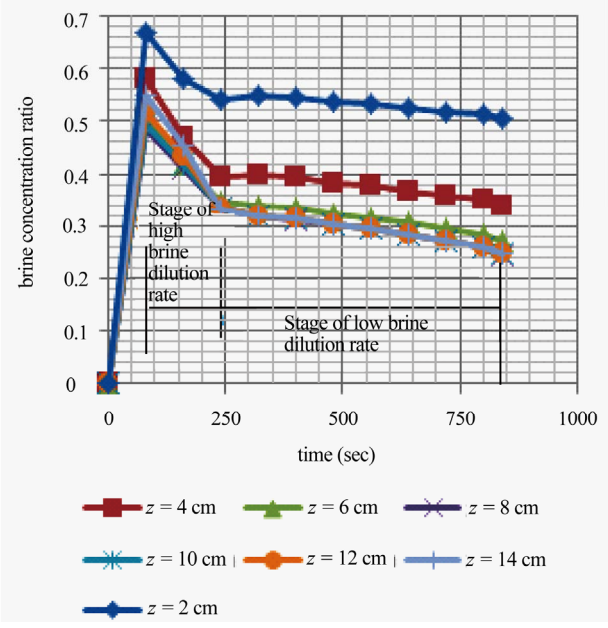

Figure 15. The breakthrough curves for brine concentration at heights from 0cm to 14 cm (maximum pentration depth = 29.2 cm).

Figure 16 presents the numerically estimated breakthrough curves for the farthest points from the port (points located from 16cm to 28 cm above the port). The numerical model produces multipeak or dual breakthrough curves where two or more brine peak concentration values take place. The existence of the dual peak concentration values reflects the eddy structures that are governed by limited extent and boundaries of the water volume around the port. It also indicates the existence of different time scales and thus different eddy scales. In other words, the existence of the second peak could be justified as follow: Once the time of the first peak has reached, entrainment of water with zero brine concentration results in jet dilution and thus reduction of the concentration peak with the course of time until the jet starts to re-entrain brine-water mixture, which cause the concentration to increase again and so on, refer to **Figure 17**.

7.5. The Vertical Brine Concentration Profile

One of the adventages of using the numerical simulation in such study is the ability to develop the breachthrough curve for the brine at a certain location. **Figure 18** illustrates a typical brine concentration calculated at the center of the inlet pipe for numerical run No. 5, where the brine concentration considerably decreases in a short vertical distance from the port then it reduces very slightly along the brine height finally it rapidly decreases

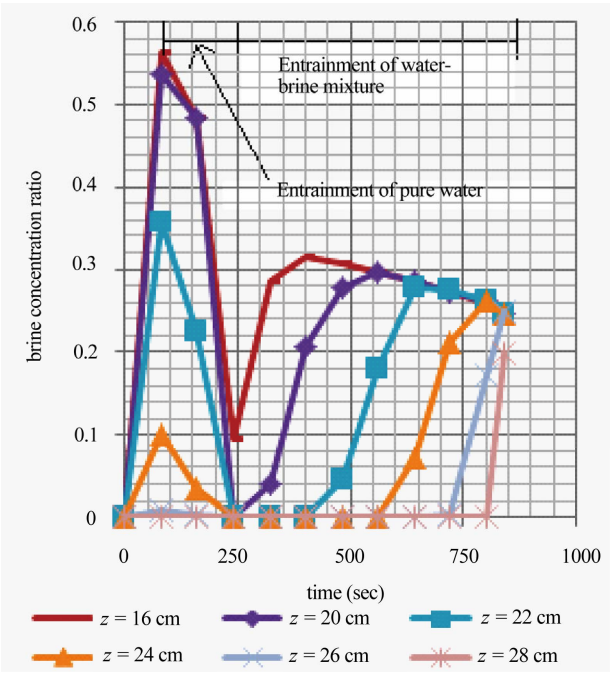

Figure 16. The multipeak breakthrough curves for brine concentration at heights from 16 cm to 28 cm (maximum pentration depth = 29.2 cm).

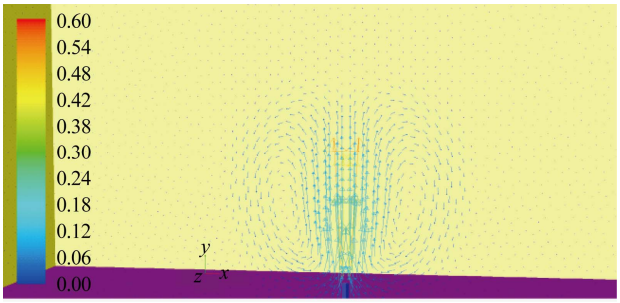

Figure 17. Schematic presentation of re-entrainment process.

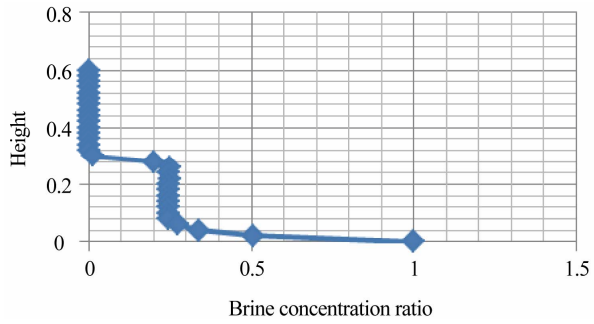

Figure 18. The vertical concentration profile (penetration height = 0.292 m, Numerical Run No. 5), v = 0.5834 m/s, d = 0.1 m & density = 1.00736 ρ_w.

till it vanishes.

8. Conclusions

This study concerns the experimental as well as numerical investigation of the buoyant dense jet that comes out from the disposal of the brine water via the desalination plants' outfalls. The work in this paper is divided into two stages. In the first stage, experimental investigation has been conducted, based on that a new empirical formula describing the penetration depth (the terminal height of rise) of dense jets is presented. The analysis of the measurements from current experiments and data from previous works confirm the validity of the linear penetration depth function in terms of the densimetric Froude number. Upper and lower envelops have been also identified for this linear formula.

In the second stage, a number of 3D numerical runs, using Fluent CFD package, has been conducted for similar conditions. Comparison of the numerical results and the empirical trends shows that the numerical model results generally agree well with the empirical investigations. The numerical simulation has revealed the existence of multipeak or dual breakthrough curves for the brine concentration. Having multipeaks of brine concentration is explained due to the limited extent of the water volume around each port.

9. Acknowledgements

The authors would like to thank Dar Al-Handasah, "Shair and partners", Resource & Environment Department, for their great and continuous support.

REFERENCES

[1] S. Matthews, "Desalination in Middle East Set to Grow," Home/Utilities Middle East, 5 April 2009.

[2] A. Purnama and H. H. Al-Barwani, "Spreading of Brine Waste Discharges into the Gulf of Oman," Desalination, Vol. 195, No. 1-3, 2006, pp. 26-31. doi:10.1016/j.desal.2005.09.036

[3] Chevron, "Reverse Osmosis Brine Disposal via Ocean Outfall Environmental Management and Monitoring Plan," G1-NT-REPX0001483, Chevron Australia Pty Ltd, 2010, p. 101.

[4] T. Bleninger and G. H. Jirka, "Modelling and Environmentally Sound Management of Brine Discharges from Desalination Plants," *Desalination*, Vol. 221, No. 1-3, 2008, pp. 585-597. doi:10.1016/j.desal.2007.02.059

[5] I. Alameddine and M. El-Fadel, "Brine Discharge from Desalination Plants: A Modeling Approach to an Optimized Outfall Design," *Desalination*, Vol. 214, No. 1-3, 2007, pp. 241-260. doi:10.1016/j.desal.2006.02.103

[6] P. J. W. Roberts and G. Toms, "Inclined Dense Jets in Flowing Current," *Journal of Hydraulic Engineering*, Vol. 113, No. 3, 1987, 232-341. doi:10.1061/(ASCE)0733-9429(1987)113:3(323)

[7] S. Latteman and T. Höpner, "Seawater Desalination: Impacts of Brine and Chemical Discharge on the Marine Environment," Balaban Desalination Publications, Italy, 2003.

[8] R. Einav, K. Harussi and D. Perry, "The Footprint of the Desalination Processes on the Environment," *Desalination*, Vol. 152, 2002, pp. 141-154. doi:10.1016/S0011-9164(02)01057-3

[9] T. N. Green, A. G. I. Dalvi and M. A. Javeed, "Chlorophyll and Plankton of the Gulf Coastal Waters of Saudi Arabia Bordering a Desalination Plant," *Desalination*, Vol. 154, No. 3, 2003, pp. 291-302. doi:10.1016/S0011-9164(03)80044-9

[10] H. Zhang and R. H. Baddour, "Maximum Penetration of Vertical Round Dense Jets at Small and Large Densimetric Froude Numbers," Journal of Hydraulic Engineering, ASCE, Vol. 124, No. 5, 1998, pp. 550-553.

[11] A. Purnama, H. H. Al-Barwani, and M. Al-Lawatia, "Modeling Dispersion of Brine Waste Discharges from a Coastal Desalination Plant," *Desalination*, Vol. 155, No. 1, 2003, pp. 41-47. doi:10.1016/S0011-9164(03)00237-6

[12] S. Shahatto, "Environmental Impact of Development in Coastal Areas: Desalination," Ph.D. Thesis, Centre for Applied Geosciences, University of Tübingen, Germany, 2003.

[13] P. J. W. Roberts and R. Sternau, "Mixing Zone Analysis for Coastal Wastewater Discharge," *ASCE Journal of En-*

vironmental Engineering, Vol. 123, No. 12, 1997, pp. 1244-1250.

[14] A. Cipollina, A. Brucato, F. Grisafi and S. Nicosia, "Bench Scale Investigation of Inclined Dense Jets," *ASCE Journal of Hydraulic Engineering*, Vol. 131, 2005, pp. 1017-1022. doi:10.1061/(ASCE)0733-9429(2005)131:11(1017)

[15] J. S. Turner, "Jets and Plumes with Negative or Reversing Buoyancy," *Journal of Fluid Mechanics*, Vol. 26, 1966, pp. 779-792.

[16] G. Abraham, "Jets with Negative Buoyancy in Homogeneous Fluids," *Journal of Hydraulic Research*, Vol. 5, No. 4, 1967, pp. 235-248.

[17] K. Cederwall, "Hydraulics of Marine Wastewater Disposal," hydraulic Division, Chalmers Institute of Technology, Gutenberg, Sweden, Report No .42, 1968.

[18] L. N. Fan and N. H. Brooks, "Numerical Solutions of Turbulent Buoyant Jet Problems," Report No. KH-R-18, California Institute of Technology, W. M. Keck Laboratory, Pasadena, California, 1969.

[19] M. A. Zeitoun, W. F. Mcllhenny and R. O. Reid, "Conceptual Designs of Outfall Systems for Desalination Plants," Report No. 550, Office of Saline Water, US Department of Interior, Washington DC, 1970.

[20] F. M. Holly and A. M. Jr., "Model Study of Dense Jets in Flowing Fluid," *ASCE Journal of Hydraulic Division*, Vol. 98, No. 11, 1972, pp. 1921-1933.

[21] V. H. Chu and M. B. Goldberg, "Buoyant Forced Plumes in a Cross Flow," *ASCE Journal of Hydraulic Division*, Vol. 100, No. 9, 1974, pp. 1203-1214.

[22] S. S. Tong and K. D. Stolzenbach, "Submerged Discharge of a Dense Effluent," Report No. 243, Ralph M Parsons laboratory, Massachusetts Institute of Technology, Cambridge, 1979.

[23] W. P. James, I. Vegara and K. Kim, "Dilution of a Dense Vertical Jet," *ASCE Journal of Environmental Engineering*, Vol. 109, No. 6, 1983, pp. 1273-1283.

[24] T. N. Mcllelan and R. E. Randall, "Measurement of Brine Jet Height and Dilution," *ASCE Journal of Waterway, Port, Coastal and Ocean Engineering*, Vol. 112, No. 2, 1986, pp. 199-204.

[25] R. M. El-Damak, M. F. Helwa and Y. R. Marmoush, "Release of Heavy Wastewater into Aquatic Environment, Experimental Investigation," Journal of Engineering, Faculty of Engineering, Cairo University, 1990.

[26] P. J. W. Roberts and G. Toms, "Inclined Dense Jets in Flowing Current," *Journal of Hydraulic Engineering*, Vol. 113, No. 3, 1987, 232-341. doi:10.1061/(ASCE)0733-9429(1987)113:3(323)

[27] H. Zhang and R. H. Baddour, "Maximum Penetration of Vertical Round Dense Jets at Small and Large Densimetric Froude Numbers," *ASCE Journal of Hydraulic Engineering*, Vol. 124, No. 5, 1998, pp. 550-553.

[28] A. Pantokratoras, "Vertical Penetration of Heated Water Jets Discharged Downwards," *ASCE Journal of Environmental Engineering*, Vol. 125, No. 4, 1999, pp. 389-392.

[29] M. E. Abou-El-Haggag, "Environmental Assessment of Brine Disposal via Marine Outfalls," Master Thesis, Faculty of Engineering, Cairo University, 2005.

[30] Fluent Manual for the ANSYS Release 12.1.4, ANSYS Inc., 2009.

[31] "Gambit 2.3 User's guide," Ansys Release, ANSYS Inc., 2006.

Notations

B_o The buoyancy flux,
C The brine concentration at any height from the port
C_o The experimental constant,
C_m The experimental constant,
C_p The brine concentration at the port.
C_r The concentration ratio = C/C_p
f The drag function,
$\boldsymbol{F}_{lift,q}$ Lift force,
$\boldsymbol{F}_q$ External body force,
F_r The jet densimetric Froude number,
$\boldsymbol{F}_{vm,q}$ Virtual mass force,
$\boldsymbol{g}$ The acceleration due to gravity,
M_o The momentum flux,
$\dot{m}_{pq}$ The mass transfer from the p^{th} to q^{th} phase,
p The pressure shared by all phases,
p_s The s^{th} solids pressure,
q The phase,
Q_o The jet outlet mass flux,
r The radius of the jet port,
$\boldsymbol{R}_q$ Interaction force between phases,
τ_p The particulate relaxation time,
$\bar{\bar{T}}_q$ The q^{th} phase stress-strain tensor,
V The fluid average velocity,
$\boldsymbol{V}_q$ The volume of phase q,
Z_m The maximum vertical penetration,
α_q q^{th} fluid's volume fraction in the cell,
$\boldsymbol{\upsilon}_q$ The velocity of phase q,
$\boldsymbol{\upsilon}_{pq}$ The interphase velocity,
λ_q Bulk viscosity of phase q,
μ_q Shear viscosity of phase q,
ρ_q The physical density of phase q,
$\hat{\rho}_q$ The effective density of phase q.
ρ_a The density of the ambient fluid &
$\Delta\rho$ The density difference between the ambient fluid and the jet.

